

Real-time modal control implementation for adaptive optics

**Allan Wirth, Joseph Navetta
Adaptive Optics Associates
54 CambridgePark Drive
Cambridge, MA 02140**

**Douglas Looze
University of Massachusetts,
Amherst, MA**

**Stefan Hippler, Andreas Glindemann,
Donald Hamilton
Max-Planck-Institut für Astronomie
Heidelberg, Germany**

Keywords: adaptive optics, wavefront reconstruction, modal control, real-time control

Abstract

This paper presents the electronics, computing hardware, and computing used to provide real time modal control for a laser guide star adaptive optics system. This approach offers advantages in the control of unobserved modes, the elimination of unwanted modes (e.g. tip and tilt) and automatic handling the case of low resolution lens arrays. In our two step modal implementation, the input vector of gradients is first decomposed into a Zernike polynomial modes by performing a least squares estimate. The number of modes is assumed to be less than or equal to the number of actuators. The mode coefficients are then available for collection and analysis, or for the application of modal weights. Thus the modal weights may be changed quickly without recalculating the full matrix. The control loop integrators are at this point in the algorithm.

To calculate the DM drive signals, the mode coefficients are converted to the zonal signals via a matrix multiply. When the number of gradients measured is less than the number of actuators, the integration in the control loop will be done on the lower resolution grid to avoid growth of unobserved modes. These low resolution data will then effectively be interpolated to yield the DM drive signals.

1. Overview

Adaptive Optics Associates (AOA) undertook a project to build a closed loop adaptive optics system for the Max Planck Institute for Astronomy at Heidelberg (MPIA). This effort was part of the Adaptive-Optics with Lasers for Astronomy (ALFA) project at MPIA. This task is unusual not for its technology but rather for the maturity of adaptive optics components to be integrated into a system for a fixed cost. The technical requirements of the adaptive optics (AO) system were such that it needed to provide flexibility over expected operating conditions such as the number of subapertures, wavefront sensor frame rate, and total closed loop bandwidth. For a detailed discussion of the application of adaptive optics to atmospheric compensation systems and a review of the configuration of “standard” systems please refer to Beckers¹.

A real-time digital wavefront computer (RTC) was built for this project to satisfy all the above requirements. Among many operating features is its capability to perform modal control of the deformable mirror within all imposed operating requirements. The division of the real-time computation will be presented along with some of the features of the software that were written for this processor. We will also show how the RTC fits into the overall control of the AO system, and how wavefront data can be collected at full frame rate for five seconds or sampled in real time for subsequent off-line processing. Modal weights for spatial filtering can be then computed for use in the RTC.

2. Adaptive Optics system requirements

The MPIA adaptive optics system is a sodium beacon laser guide star system to be installed on a 3.5m telescope in Calar Alto, Spain. Technical details of the system have been presented elsewhere², and we will review the requirements pertinent to the fabrication of the RTC. Figure 1 shows an electrical layout of the adaptive optics system. The components of the RTC are given within the box at the upper left. Also shown are the major electrical and communications connections. The shaded components were supplied by MPIA for integration. The remaining components were either procured or built by AOA.

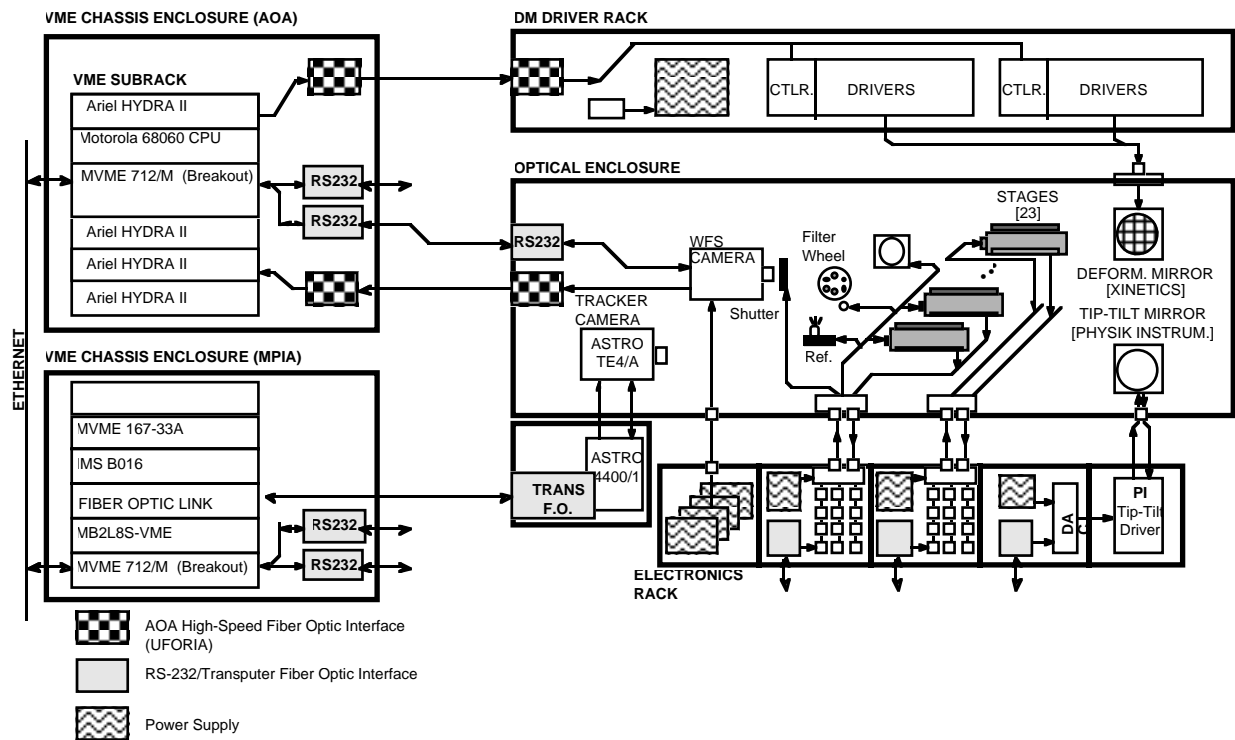


Figure 1: Functional layout of the electrical system for the MPIA AO system.

2.1 Functional requirements of system

The table below shows part of the requirements for this adaptive optics system. Although the number of actuators is fixed, the number of subapertures driving them may be varied from as few as 6 to as many as 100. The geometry of the projected subapertures over the telescope pupil is given in Figure 2. In cases where there are many fewer subapertures than actuators, some interpolation scheme needs to be employed to derive actuator commands. One method is to model the wavefront of turbulence in terms of Zernike polynomials^{3,4}, which forms the basis of our implementation in the RTC.

Table 1: Summary of requirements for MPIA adaptive optics system.

<u>Attribute</u>	<u>Specification</u>
DM actuators	97
Subapertures	100, 72, 48, 18, 6
Wavefront sensor frame rates	$100 \leq f \leq 1200$ Hz
Closed loop bandwidths	≤ 100 Hz

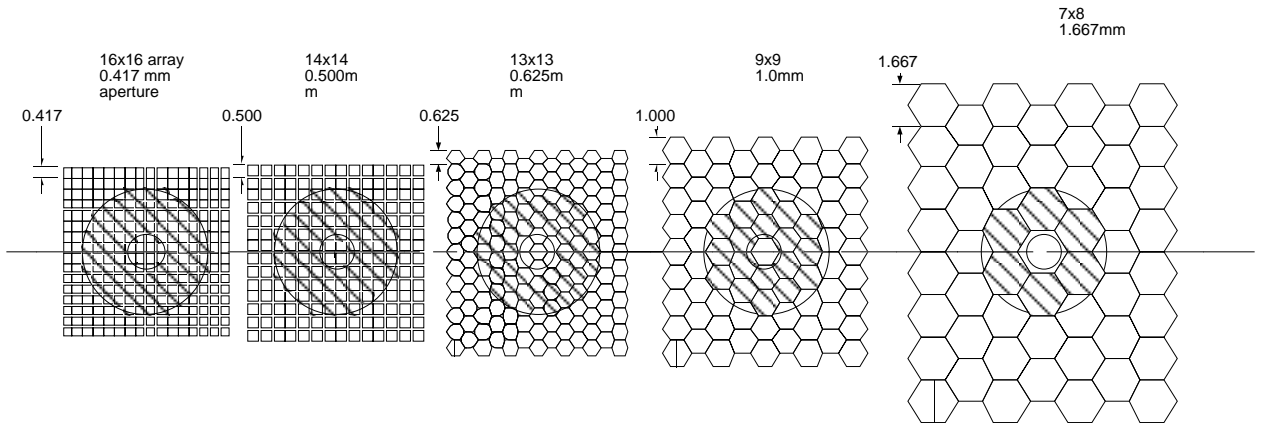


Figure 2: Shack-Hartmann wavefront sensor configurations for MPIA adaptive optics system. All arrays on a single substrate, epoxy replicas on glass. Shaded lenslets represent active subapertures.

3. Modal Control Architecture and Design

3.1 Introduction

The objective of this section is to present the logical architecture and algorithm design for the ALFA adaptive optics system. The logical architecture employs a standard design with separate tip-tilt and deformable mirror control loops. The tip-tilt control loop was implemented using an existing tip-tilt control system developed by MPIA ⁵. The deformable mirror (DM) control loop uses a modal compensation technique.

The objective of the modal compensation approach is to use actuator patterns that implement spatial mode shapes to attenuate the energy contained in those modes within the optical wavefront. The more traditional zonal approach attempts to attenuate the phase aberrations in the optical wavefront at the locations of the deformable mirror actuators.

Several factors contributed to the selection of the modal approach for the ALFA adaptive optics system. First, it was anticipated that the coarser lenslet arrays would often be in

use due to the limited available light. Only the finest lenslet array provides a sufficient number of gradient measurements to be able to possibly reconstruct the phase at each aperture. Second, even with the finest lenslet array, the geometry of the ALFA optical path prevents the corners of the subapertures from being aligned with the actuators (see Figure 3). In fact, some of the actuator locations are near the center of a subaperture, which causes their effect to be almost unobservable. Also, several of the coarser arrays have hexagonal shapes that further complicate the association of corner phase values with actuators. Finally, the modal approach allows the lenslet arrays to be interchanged with virtually no adjustment to the rest of the DM control system. Although these factors do not preclude a form of zonal compensation from being implemented, the modal approach led to a simpler and more flexible design.

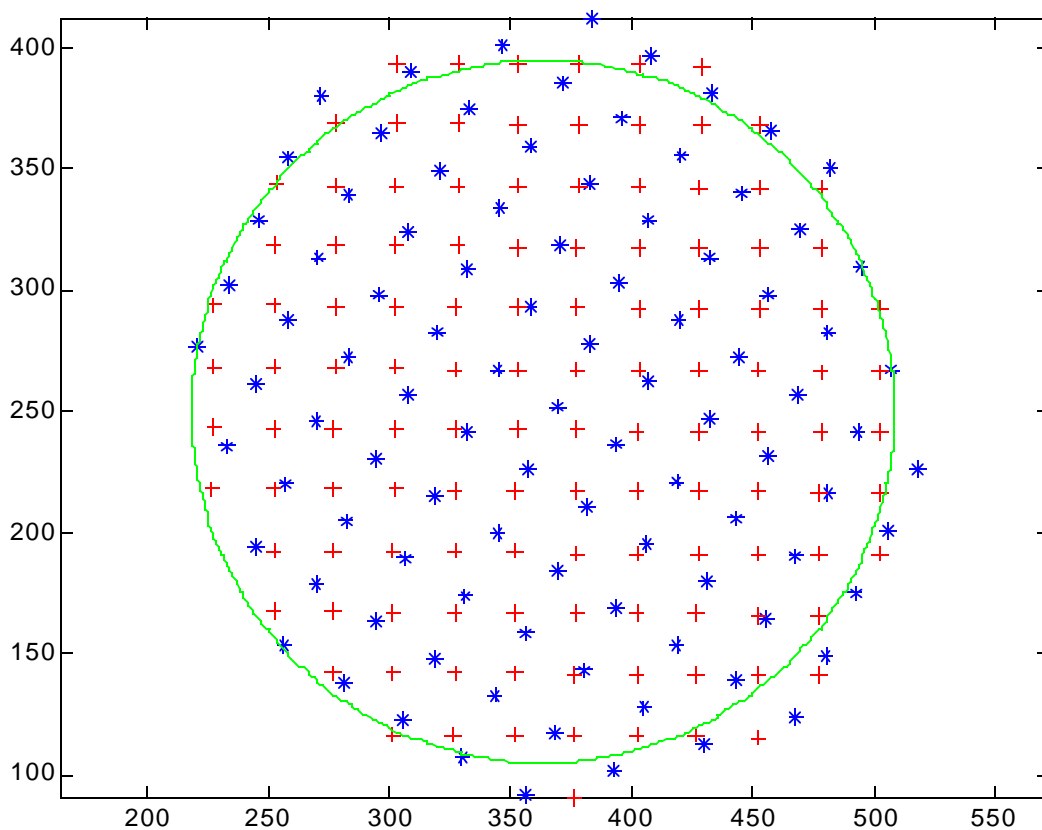


Figure 3. Superposition of the wavefront sensor view of the actuator positions (*), subaperture centers for the finest lenslet array (+), and aperture for the geometry of the ALFA optical system. The axis scales are in image pixels.

The remainder of this section is organized as follows. The architecture and interactions of the ALFA control loops are discussed in Section 3.2. The specification and design of the individual DM control system functions is presented in Section 3.3. Results of the ALFA adaptive optics from both laboratory testing and operation on the Calar Alto 3.5 m telescope are given in Section 3.4.

3.2 Adaptive Optics Control System Architecture

3.2.1 Overall Architecture

The ALFA adaptive optics system employs a standard logical control architecture that decomposes the control system into two separate, ideally non-interacting loops (see Figure 4). The tip-tilt control loop measures the full aperture tip and tilt of the incoming wavefront and attempts to remove any detected tip or tilt by driving the tip-tilt mirror. The DM control loop measures all other aberrations in the wavefront, and attempts to remove them by appropriately shaping the deformable mirror.

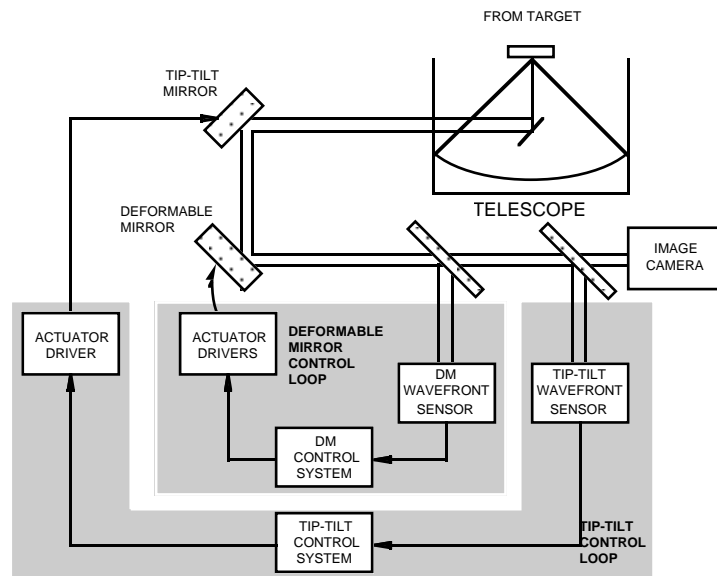


Figure 4. Logical control architecture of the ALFA adaptive optics system.

3.2.2 Tip-Tilt Control System Architecture

The tip-tilt control loop is a control system design and implementation developed by MPIA. The logical organization of the tip-tilt control system is shown in Figure 5. The full aperture tip and tilt measurements are obtained from the tip-tilt camera. These measurements are then compensated using a proportional-plus-integral control algorithm. The compensated tips and tilts are then transformed into actuator commands that are applied to the tip-tilt mirror.

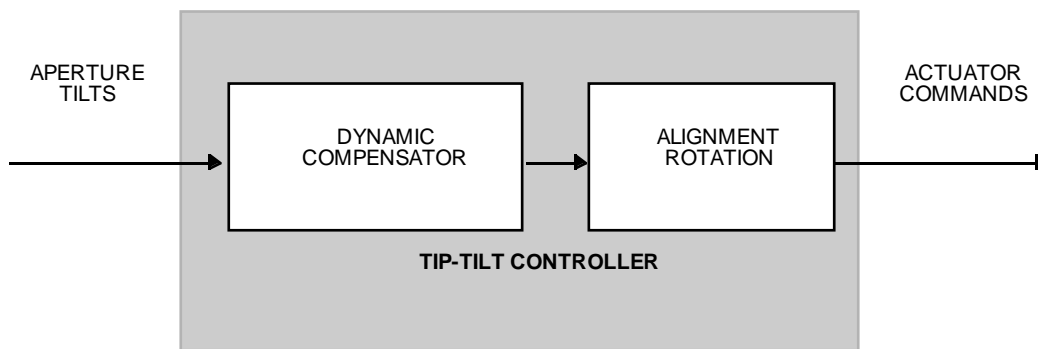


Figure 5. Logical control architecture of the tip-tilt control loop.

The frequency of operation of the tip-tilt camera can be set by the observer, with a maximum frequency of 100 Hz. Operation on the Calar Alto 3.5 m telescope typically uses an 80 Hz frame rate. The control algorithm parameters are fixed, and provide a disturbance rejection bandwidth of approximately 1/15 the frame rate. Thus, full aperture tip and tilt aberrations are attenuated up to about 5 Hz during normal operation at the Calar Alto observatory. Details of the design and operation of the tip-tilt control loop can be found in ref. 4.

In an alternative configuration the tip-tilt signals are derived from the wavefront sensor data and thus are available at the same frame rate as the higher order wavefront estimations. This mode is useable only for natural guide star operation because the laser guide star does not yield valid tilt information.

3.2.3 Deformable Mirror Control System Architecture

The logical control architecture of the DM control system is shown in Figure 6. The subaperture gradients are local gradients of the phase of the incoming wavefront, as measured

by the Hartmann sensor. Given a set of spatial modes to be compensated, the modal reconstructor uses the subaperture gradients to determine the coefficients the modes that are present in the wavefront. These modal coefficients can be adjusted by applying an offset. These offsets are available to allow for the compensation of known differences between the modal estimate and the true wavefront error. An example of this is the focus error due to the zenith distance dependence of the range to the sodium layer. In that case an open loop focus offset calculated from the zentih angle is applied to prevent drift in the image focus for stellar objects. The dynamic compensation of the modal coefficients is designed to attenuate each of the modes that is being compensated. The compensated modal coefficients are then multiplied by the modal injector to generate actuator commands that will produce the corresponding modal pattern on the surface of the DM.

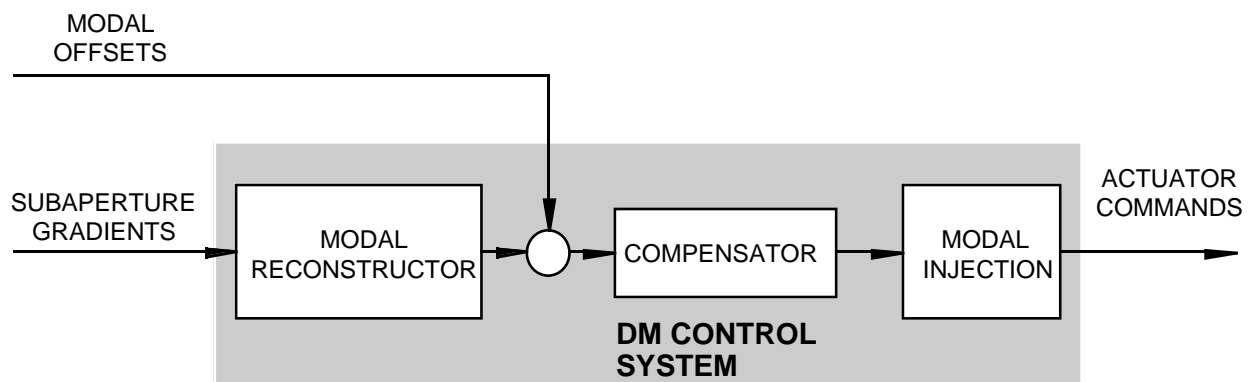


Figure 6. Logical control architecture of the deformable mirror control system.

The logical architecture of the more standard zonal approach to adaptive optics design is virtually identical to that shown in Figure 6. In the zonal approach, the reconstructor attempts to compute the phase of the wavefront at the actuator locations. Each local phase is then compensated, and the compensated phase is used directly to drive the actuators. The only modification required to the architecture of Figure 6 is that the modal injection function becomes an identity (i.e., a direct feedthrough of the compensated phases to the actuator drives). In fact, the zonal approach can be regarded as a special case of the modal approach in which the modes to be compensated are spatial point functions at the actuator locations.

3.3 Design of the DM Control System Function

3.3.1 Modal Approach to the Deformable Mirror Control Problem

Figure 7 contains a block diagram representation of the principal elements of the deformable mirror feedback loop of the ALFA adaptive optics system. The principal components of the system are the deformable mirror, the wavefront sensor, the modal reconstructor, the dynamic modal compensation system, and the modal injection system. The function of the block that represents the deformable mirror in the feedback loop is to map the applied controls into a modified mirror surface s . The incident wavefront (including the atmosphere induced aberration d) is reflected off the surface to produce the reflected wavefront e . The phase of the reflected wavefront is the sum of the phase variation induced by atmospheric aberrations of the incident wavefront d and the phase variation induced by the deformed mirror surface. Thus the atmospheric wavefront aberrations are represented as additive disturbances.

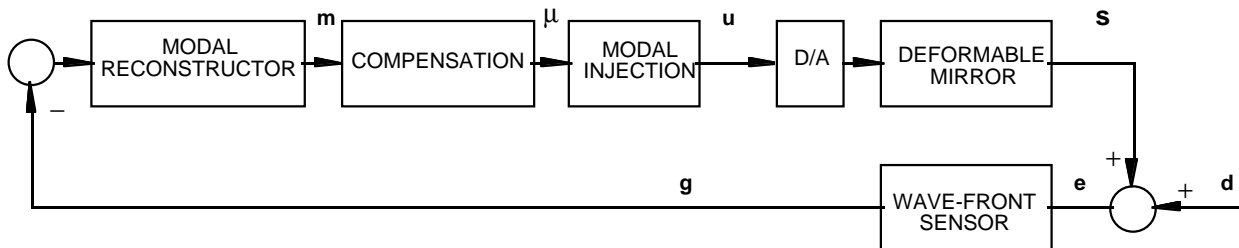


Figure 7. Block diagram of the feedback loop of the deformable mirror.

Physically, the wavefront aberrations d , the effect of the deformed mirror surface s , and the reflected wavefront e are distributed signals with continuous spatial and temporal variations. As viewed by the wavefront sensor, these signals will be denoted by $d(x, y)$, $s(x, y)$ and $e(x, y)$ respectively, where the z -axis is taken to be along the optical path, and the x -axis and y -axis define the viewing plane of the sensor. The relationship between these signals is:

$$e(x, y) = s(x, y) + d(x, y)$$

It will be assumed that each of the signals belongs to a Hilbert (inner product) space H of functions defined on the aperture disk A as viewed by the wavefront sensor, with inner product:

$$\langle \mathbf{a}, \mathbf{b} \rangle = \int_A \mathbf{a}(x, y) \mathbf{b}(x, y) dx dy$$

The resulting wavefront error vector $\mathbf{e}(x, y)$ is measured by the wavefront sensor. The wavefront sensor measures an approximation to the average x and y slopes of the phase over the subaperture. For the purposes of designing the DM control system functions, it will not be necessary to determine the precise relationship between the gradient measurements produced by the wavefront sensor and the wavefront phase $\mathbf{e}(x, y)$. We will only assume that this relationship is linear. Hence, the gradient vector \mathbf{g} which consists of the x and y subaperture gradient measurements is assumed to be given by:

$$\mathbf{g} = W(\mathbf{e}) \tag{1}$$

where $W(\bullet)$ is a linear operator. The response of the sensor to input gradients was measured and found to be quite linear over a large dynamic range. This linearity was achieved in part by using between 25 and 200 pixels to measure the Hartmann spot position in each subaperture. The negative effects that these large numbers of pixels can have on noise performance were largely eliminated by the use of a matched filter algorithm to estimate spot locations. This algorithm uses only well illuminated pixels near the spot center to produce its estimate. The wavefront sensor operates at a user selected frame rate between 100 Hz and 1200 Hz.

The deformable mirror maps the actuator commands \mathbf{u} into a deformed mirror surface \mathbf{s} . We will assume that the steady-state relationship between the mirror surface and the actuator commands is linear. Thus,

$$\mathbf{s} = M(\mathbf{u}) \tag{2}$$

where $M(\bullet)$ is a linear operator.

It will also be assumed that the steady-state mirror surface at the actuator positions is deformed proportionally to the actuator command at that position. That is, let $\{(x_{ai}, y_{ai})\}_{i=1}^{N_a}$ denote the N_a actuator locations (as viewed by the wavefront sensor). Then,

$$s(x_{ai}, y_{ai}) = \alpha u_i \quad i = 1, \dots, N_a \quad (3)$$

where α is a proportionality constant that is independent of the actuator.

It should be noted that this assumption does not hold exactly. In practice, an actuator command u_i will influence the mirror surface at nearby actuator locations. For the DM used in the ALFA system, this influence is less than 10% for neighboring actuators. Further, the proportionality constant α varies from actuator to actuator. This variation in response was measured using a high accuracy Hartmann sensor and found to be on the order of $\pm 10\%$ except for edge actuators. As long as the actuator commands produce a relatively smooth surface, equation (3) will be approximately satisfied.

3.3.2 Injection Matrix

Let $\{\mathbf{Z}_{n,m}(\rho, \theta) : n = 0, \dots, \infty; m = -n, -n + 2, \dots, n\}$ denote the set of Zernike polynomials defined on the wavefront aperture image A , where the radius ρ and angle θ represent the standard transformation from x and y coordinates. Any incident wavefront \mathbf{d} can be represented in terms of these polynomials by:

$$\mathbf{d}(\rho, \theta) = \sum_{n,m} d_{n,m} \mathbf{Z}_{n,m}(\rho, \theta)$$

The surface deformation of the mirror can be represented by:

$$s(\rho, \theta) = \sum_{n,m} s_{n,m} \mathbf{Z}_{n,m}(\rho, \theta)$$

Ideally, the deformable mirror surface could be modified by specifying the actuator voltages to exactly cancel the wavefront aberration \mathbf{d} . This will be accomplished if $s_{n,m} = d_{n,m}$.

However, the finite number of actuators limits the degrees of freedom that are available to specify the mirror surface. In particular, the range of the linear operator in equation (2) will be an N_a subspace. In addition, the use of a finite number of lenslets N_l means that at most a $2N_l$ subspace can be observed. Thus the DM control system is limited to attenuating aberrations within finite dimensional subspaces of the actual signal space.

Because atmospheric aberrations have most energy in lower order modes (as indexed by n) with decreasing energy as the mode order increases, the control effort can be concentrated on attenuating the lower order sets of Zernike modes. The first two sets of modes are special: $n=0$ is the piston mode which is unobservable; and $n=1$ are the tip and tilt modes which are controlled separately by the tip-tilt control system. Thus, it will be assumed that the control objective is to attenuate the Zernike modes associated with indices $\{n\}_{n=2}^{N_c}$. Note that the use of sets of Zernikes with common radius power indices results in a circularly symmetric set of polynomials.

If equation (3) holds and if the actuator spacing is small relative to the spatial variation of the mode $\mathbf{Z}_{n,m}$, this mode can be approximately generated by applying the actuator commands:

$$\mathbf{u}_{n,m} = \begin{bmatrix} \mathbf{Z}_{n,m}(\rho_1, \theta_1) \\ \vdots \\ \mathbf{Z}_{n,m}(\rho_{N_a}, \theta_{N_a}) \end{bmatrix}$$

where $\{(\rho_i, \theta_i)\}_{i=1}^{N_a}$ are the actuator locations in radial coordinates. Let

$$\mathbf{s}_{n,m} = \mathbf{M}(\mathbf{u}_{n,m}) \approx \mathbf{Z}_{n,m} \quad (4)$$

Thus, the actuator command signal:

$$\mathbf{u} = - \sum_{n=2}^{N_c} \sum_m d_{n,m} \mathbf{u}_{n,m} \quad (5)$$

will result in the error signal:

$$\mathbf{e} = \sum_{n=2}^{N_c} \sum_m d_{n,m} (\mathbf{Z}_{n,m} - \mathbf{s}_{n,m}) + \sum_{n=N_c+1}^{\infty} \sum_m d_{n,m} \mathbf{Z}_{n,m} \quad (6)$$

Consequently, \mathbf{e} can be made small if the approximation in (4) holds and if the residual in the second summation term in (6) is small. The approximation in (4) will hold if (3) approximately holds and if the actuator separation is not too large, while the second summation in (6) will be small if enough Zernike terms are included in the controlled set. The surface figure of the DM was observed while several of the Zernike modes were applied as command sets. Residual errors relative to the theoretical polynomial shape of 5-10% were observed. Because of the technique used to generate the reconstruction matrix (see Section 3.3.3) these errors do not significantly affect the system performance.

The formula for the actuator commands (5) can be regarded as the product of a set of modal coefficients and the actuator command vectors $\{\mathbf{u}_{n,m}\}$ that “inject” the coefficient into the surface space. More generally, for a set of modal coefficients $\{\mu_{n,m}\}$, formula (5) can be written as a matrix multiplication. Define $\boldsymbol{\mu}$ to be the vector of modal coefficients and \mathbf{M} to be the matrix whose columns are the actuator command vectors:

$$\boldsymbol{\mu} = \begin{bmatrix} \mu_{2,-2} \\ \mu_{2,0} \\ \mu_{2,2} \\ \mu_{3,-3} \\ \mu_{3,-1} \\ \vdots \end{bmatrix} \quad \mathbf{M} = [\mathbf{u}_{2,-2} \quad \mathbf{u}_{2,0} \quad \mathbf{u}_{2,2} \quad \mathbf{u}_{3,-3} \quad \mathbf{u}_{3,-1} \quad \cdots]$$

Then (5) can be written:

$$\mathbf{u} = \mathbf{M}\boldsymbol{\mu} \quad (7)$$

The matrix multiplication defined by (7) is the modal injection operation in Figure 7.

While in the foregoing discussion the set of modal polynomials has been referred to as Zernike polynomials, the set used in the ALFA system is slightly modified. The Zernike focus term was retained but the higher order modes were re-orthonormalized in the actuator location

space to assure that these high-order modes are distinguishable on the mirror surface. This process lead to a progressive deviation of the polynomials from the standard Zernike set at higher spatial frequencies.

3.3.3 Modal Reconstruction

The ideal objective of the modal reconstruction operation is to determine the modal coefficients corresponding to the Zernike modes that are being controlled. Although it is possible to derive analytic relationships that relate the gradients to the Zernike modes and coefficients, the relationships would be sensitive to modeling assumptions (e.g., how are the gradient vectors related to the subaperture shapes) and to the physical alignment of the subapertures and deformable mirror.

Rather than basing the modal reconstruction on an analytic model, the ALFA DM control system uses a static identification procedure to determine the effect of applying the modal injection vectors to the deformable mirror. A laser is inserted into the optical path and used to illuminate the DM. Each of the modal injection vectors is then applied in sequence, and the static pattern of the resulting gradients is determined. These patterns are then used to compute the reconstruction matrix. This process also acts to ameliorate the effects of the “real” DM versus the ideal model assumed in creating the injection matrix. Even if the DM surface deviates from the theoretical modal shape, what is measured is the response of the sensor to the actual surface figure of the mirror. The remaining concern is that the resulting set of “real” modes is no longer orthogonal either in the actuator space or in the measurement space of the wavefront sensor. This possibility and the possibility that some of the selected modes have very low observability by the wavefront sensor were addressed by performing a sensitivity analysis of the final system. Modes that were found to have low observability or poor rejection were given low or zero weights in the reconstruction. It was found that, as a rule of thumb, the final number of modes controlled was about 2/3 of the theoretical maximum number that could be observed with a given number of subapertures.

Assume that the modal injection vector $\mathbf{u}_{n,m}$ is applied to the deformable mirror with amplitude γ . Let $\mathbf{g}_{n,m}$ denote the resulting gradients that are recorded. The mirror surface that results is given by:

$$\mathbf{s} = \gamma \mathcal{M}(\mathbf{u}_{n,m}) = \gamma \left(\mathbf{Z}_{n,m} - (\mathbf{Z}_{n,m} - \mathcal{M}(\mathbf{u}_{n,m})) \right) \approx \gamma \mathbf{Z}_{n,m}$$

That is, γ is approximately the Zernike coefficient of the DM surface deformation. Because the incident wavefront is from a laser, the wavefront error \mathbf{e} is the same as the surface deformation \mathbf{s} :

$$\mathbf{e} = \mathbf{s} \approx \gamma \mathbf{Z}_{n,m}$$

Hence,

$$\mathbf{g}_{n,m} = \gamma \mathcal{W}(\mathcal{M}(\mathbf{u}_{n,m})) \quad (8)$$

In general, if modal coefficients $\{\mu_{n,m}\}$ are applied to the deformable mirror, the surface of the mirror and the wavefront error will be:

$$\mathbf{e} = \mathbf{s} = \sum_{n=2}^{N_c} \sum_m \mu_{n,m} \mathcal{M}(\mathbf{u}_{n,m}) \approx \sum_{n=2}^{N_c} \sum_m \mu_{n,m} \mathbf{Z}_{n,m}$$

Hence, the coefficients $\{\mu_{n,m}\}$ are approximately the Zernike modal coefficients. The gradient that results from this actuator command is:

$$\mathbf{g} = \sum_{n=2}^{N_c} \sum_m \mu_{n,m} \mathcal{W}(\mathcal{M}(\mathbf{u}_{n,m})) = \sum_{n=2}^{N_c} \sum_m \mu_{n,m} \mathbf{g}_{n,m} \quad (9)$$

Define:

$$\boldsymbol{\mu} = \begin{bmatrix} \mu_{2,-2} \\ \mu_{2,0} \\ \mu_{2,2} \\ \mu_{3,-3} \\ \mu_{3,-1} \\ \vdots \end{bmatrix} \quad \mathbf{G} = \begin{bmatrix} \mathbf{g}_{2,-2} & \mathbf{g}_{2,0} & \mathbf{g}_{2,2} & \mathbf{g}_{3,-3} & \mathbf{g}_{3,-1} & \cdots \end{bmatrix}$$

Then, (9) can be rewritten:

$$\mathbf{g} = \mathbf{G}\boldsymbol{\mu} \quad (10)$$

The matrix \mathbf{G} will be left invertible if the modes that are to be controlled can be observed independently by the wavefront sensor. Assuming this is the case, the modal coefficients can be determined (reconstructed) by:

$$\boldsymbol{\mu} = \left(\mathbf{G}^T \mathbf{G}\right)^{-1} \mathbf{G}\mathbf{g} \equiv \mathbf{H}\mathbf{g} \quad (11)$$

where \mathbf{H} is the modal reconstruction matrix.

The ALFA DM control system incorporates the on-line calibration of the modal reconstruction matrix described in the preceding paragraphs. Specifically, the on-line calibration applies actuator commands corresponding to a constant modal injection vector $\mathbf{u}_{n,m}$. After any transients have died out, the gradient vector is averaged over 20 frames to obtain $\mathbf{g}_{n,m}$. The process is repeated for each mode to be controlled. The matrix \mathbf{G} is constructed, and the reconstruction matrix \mathbf{H} is computed. The identification process takes less than 2 minutes for 20 modes.

3.3.4 Compensation Algorithm

3.3.4.1 Dynamic Models

Design of the compensation algorithm requires models of the significant dynamics of the control loop. Until this point, the models that were developed for the elements of the control loop were static mappings that determined steady-state relationships between their inputs and

outputs. There are three significant sources of dynamic variations in the DM control loop that must be represented⁶. First, the DM actuators exhibit first-order dynamic responses at frequencies of interest to the adaptive optics problem. Second, the computation time required to read the CCD, construct the gradients, and compute the modal coefficients can be significant. Finally, the inherent time discretization induced by the frame rate of the wavefront sensor camera requires the system to be treated as a sampled-data system. Hence the dynamics of the D/A converter and sampling process are important.

A block diagram of the mapping from the output of the compensator algorithm (the commanded modes μ) to the input to the compensator algorithm (the reconstructed modes \mathbf{m}) is shown in Figure 8. The modal injection function contains no dynamics and is simply a matrix multiplication. The deformable mirror has first order dynamics associated with the actuators (see discussion in Ref. 5) as well as the mapping into the surface deformation defined by (2). We will model the actuator dynamics as identical for each actuator. Thus, the deformable mirror can be decomposed as shown in Figure 9. From the manufacturer specifications and laboratory measurements, the time constant of the DM actuators τ_a was determined to be:

$$\tau_a = 2 \times 10^{-4} \text{ s}$$

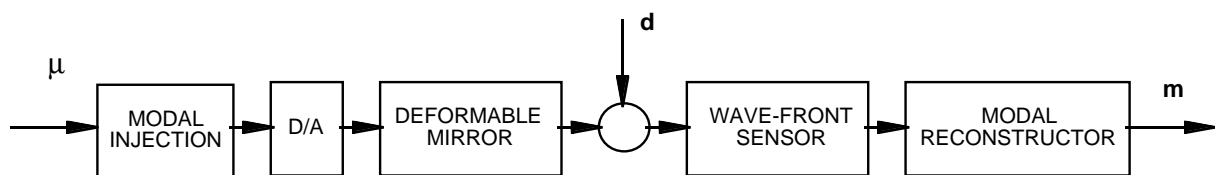


Figure 8. Mapping from compensated modes to reconstructed modes.

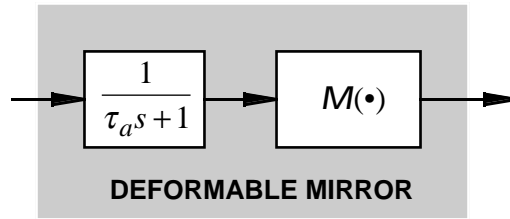


Figure 9. Dynamical model of the deformable mirror.

The wavefront sensor can be modeled as three separate functions (see Figure 10): the static mapping between the wavefront error \mathbf{e} and the gradients given by (1); the sampling of the wavefront due to the camera frame rate; and the time delay due to the computation of the gradients and reconstructed modes. Note that the last element could be broken into the two separate delays associated with the gradient computation and camera readout, and the modal reconstruction. Because the effects of these delays are identical as far as the compensation algorithm is concerned, they will be treated as one.

As discussed in [ID], it is reasonable to assume that the wavefront sensor/reconstructor delays are identical in all channels. Based on a timing diagram of the computations and laboratory measurements, the effective delay τ_c was found to be:

$$\tau_c = 1.5 \times 10^{-3} \text{s}$$

Because the computation time associated with the modal reconstruction was included in the wavefront sensor, the modal reconstruction is represented as a matrix multiplication given by (11).

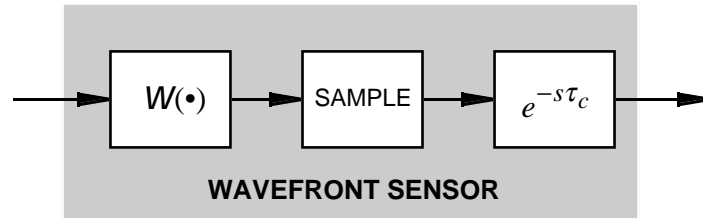


Figure 10. Dynamical model of the wavefront sensor.

The overall block diagram including the significant dynamic effects is shown in Figure 11. This model can be simplified by noting that the D/A operation and the modal injection matrix multiplications can be (for the purpose of mathematical modeling) interchanged. Similarly, the sampling operation, the modal reconstruction and the delay can be interchanged. The addition of incident wavefront signal can be moved using block diagram manipulation to the end of the blocks (see Figure 12). Finally, the static DM function, the static wavefront sensing function and the modal reconstruction can be combined using equations (8), (10), and (11):

$$\mathbf{H}(W \circ M)M = \mathbf{I}$$

The resulting dynamical model with an equivalent incident wavefront aberration \mathbf{d}' is shown in Figure 13. Note that the choice of reconstructors (11) results in a diagonal transfer function with identical dynamics when viewed from the point of the compensation algorithm.

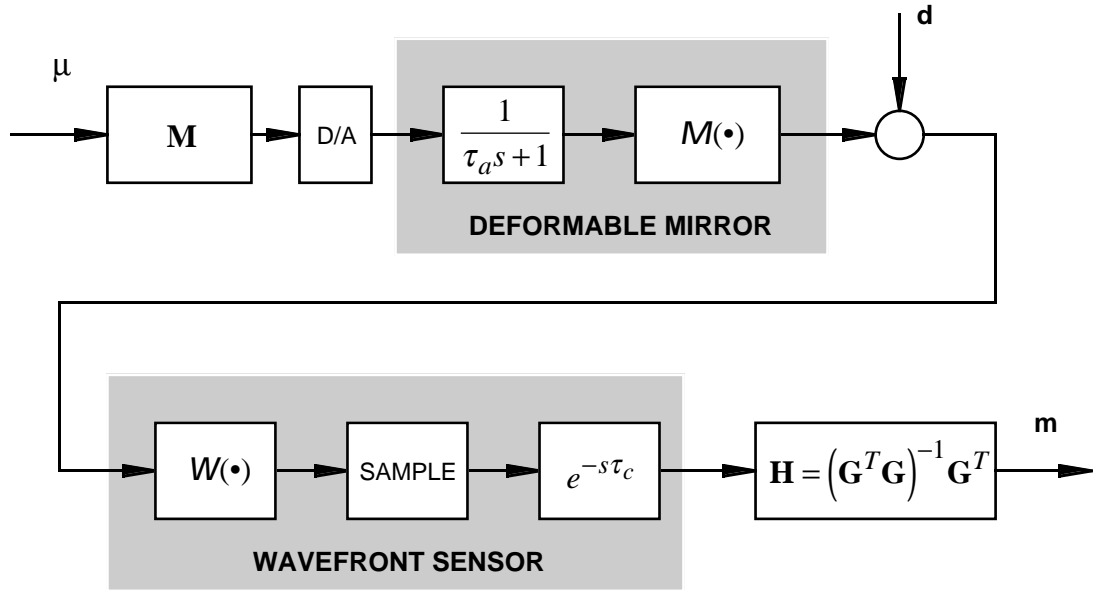


Figure 11. Adaptive optics dynamic models.

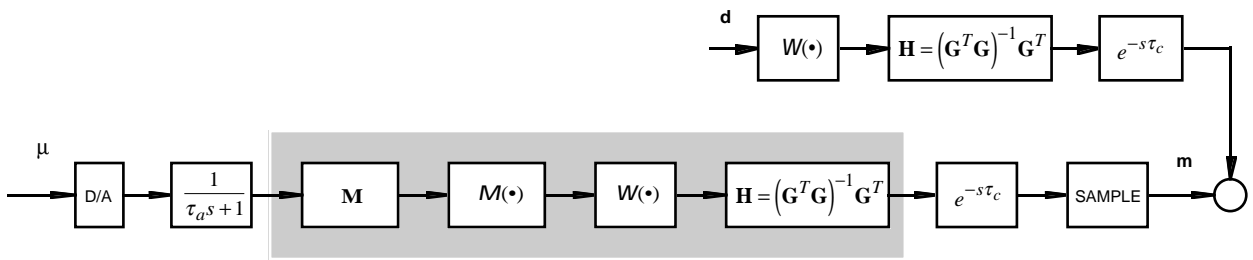


Figure 12. Adaptive optics dynamic models after manipulation

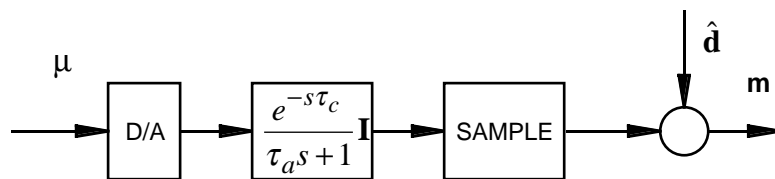


Figure 13. Simplified dynamic model.

The combination of the D/A converter, continuous-time transfer function and sampling operation can be represented as a single discrete-time transfer function^{5,7}. For a model of the form shown in Figure 13 with a sampling period of T_s , the equivalent discrete-time transfer function $\mathbf{P}(z)$ is given by:

$$\mathbf{P}(z) = \frac{(1-\delta)}{(1-\gamma)} \frac{z-\gamma}{z^l(z-\delta)} \mathbf{I}$$

where z is the complex discrete frequency variable, the order l of the pole at the origin and the zero γ are determined by the delay τ_c and the sampling period T_s , and the pole δ is determined by the continuous-time pole time constant τ_a and the sampling period T_s :

$$\begin{aligned} \gamma &= (\exp(-T_s / \tau_a) - \exp(\tau_c / \tau_a)) / (1 - \exp(\tau_c / \tau_a)) \\ \delta &= \exp(-T_s / \tau_a) \end{aligned}$$

3.3.4.2 Compensator Design and Performance

Because the transfer function $\mathbf{P}(z)$ is diagonal with identical dynamics, the compensator design for each modal coefficient can be the same. Hence the compensation algorithm design can be developed using single-input, single-output techniques (see ref 6). The overall closed-loop system viewed from the compensation algorithm is shown in Figure 14.

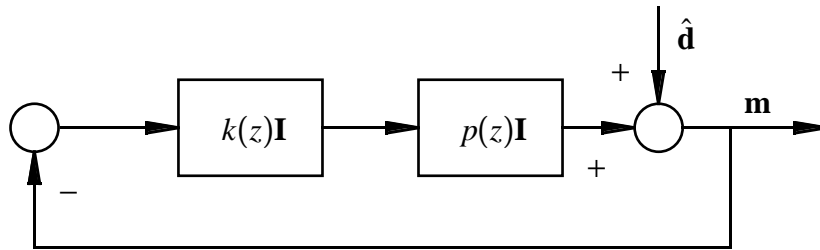


Figure 14. Compensation loop block diagram.

Although there are other errors that can affect the modal coefficients (such as measurement noise and modeling errors), the dominant uncertainty is the incident wavefront aberrations represented by $\hat{\mathbf{d}}$. Thus, the objective of the compensation design is to attenuate the

influence of the effective disturbance $\hat{\mathbf{d}}$ on the modal coefficients \mathbf{m} . From Figure 14, the modal coefficients are given by:

$$\mathbf{m} = \frac{1}{1 + p(z)k(z)} \mathbf{Id}' = S(z)\mathbf{Id}'$$

where $S(z)$ is called the sensitivity function.

The modal coefficients will be small if the sensitivity function is small at frequencies for which the disturbance (i.e., the atmospheric aberrations) are large. The sensitivity function can be made small by making the compensation transfer function $k(z)$ large. However, to maintain stability, the compensator must be small at high frequencies (approaching the sampling frequency). This is often accomplished by using a proportional-plus-integral (PI) controller. In our case, the presence of potentially significant phase delays in the transfer function $p(z)$ requires additional lead compensation. The general form of the compensator was thus selected to be:

$$k(z) = k_0 \left(\frac{z - \alpha}{z - 1} \right) \left(\frac{z - b}{z - a} \right) \left(\frac{1 - a}{(1 - \alpha)(1 - b)} \right) \quad (12)$$

The first factor is the PI compensation, the second term allows for additional lead compensation, and the last term normalizes the gain of the factors. The overall compensator gain is determined by k_0 .

The individual parameters were determined for several wavefront camera frame rates using a combination of frequency domain compensation and root-locus methods. The parameters for each of the frame rates considered are shown in Table 2. Bode plots of the magnitudes of the sensitivity function are shown in Figure 15 for the frame rates of 300 Hz and 1200 Hz. Note that the disturbance rejection bandwidth in each case is approximately 1/12 of the frame rate in Hz, and that the sensitivity peak in each case is approximately 6 db. Also, the design parameters for all designs below 600 Hz are identical because the phase lags from the actuator dynamics and computations are almost insignificant at those frequencies. The additional lead compensation term in (12) is only needed for the 900 Hz and 1200 Hz designs.

Table 2. Compensation parameters and disturbance rejection bandwidth for various wavefront sensor camera frame rates.

Frame Rate	k_0	α	a	b	Bandwidth
100 Hz	0.5	0.2	0.0	0.0	8 Hz
200 HZ	0.5	0.2	0.0	0.0	16 Hz
300 Hz	0.5	0.2	0.0	0.0	24 Hz
600 Hz	0.5	0.2	0.0	0.0	32 Hz
900 Hz	0.5	0.2	-0.2	0.0	75 Hz
1206 Hz	0.5	0.3	-0.7	0.0	100 Hz

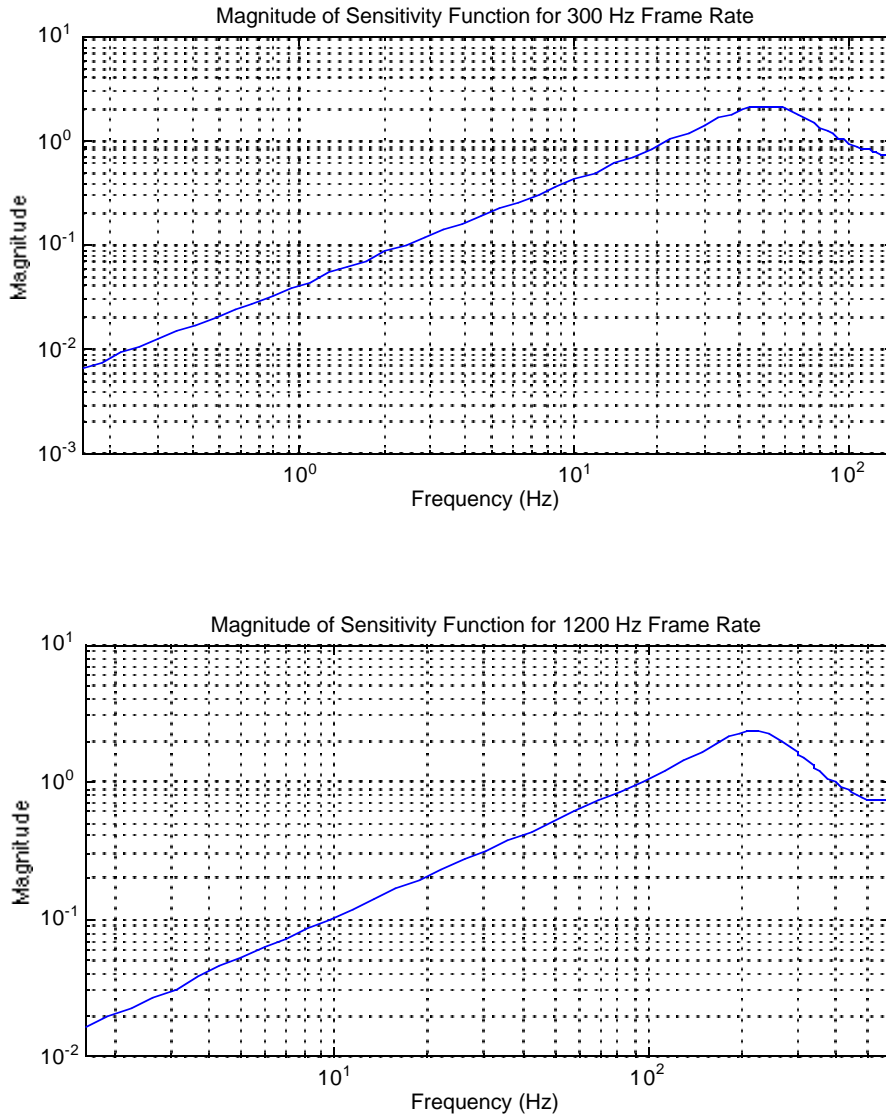


Figure 15. Magnitudes of sensitivity function for 300 Hz and 1200 Hz designs.

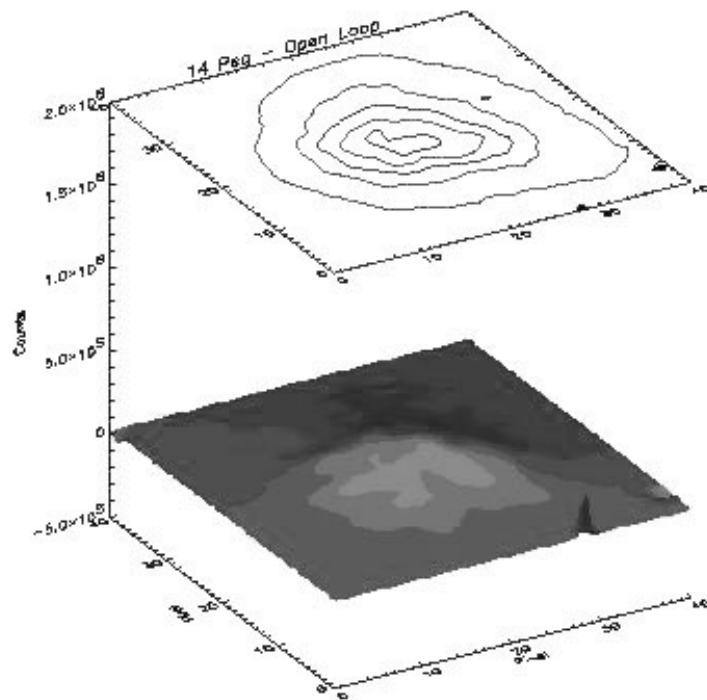
3.4 Results

The ALFA adaptive optics system was installed on the 3.5 m telescope at the Calar Alto Observatory in Spain in September, 1996. Stable operation of the adaptive optics loops was achieved from the beginning. A small selection of recent results are presented here. For the latest information please refer to the ALFA site on the internet at:

www.mpia-hd.mpg.de/MPIA/Projects/ALFA.

Several stars in the range 4-6 magnitude were observed using wavefront camera frame rates up to 900Hz with the parameters from Table 2 and the tip-tilt loop operating at 80 Hz frame rate. The results from observation of 14 Peg and Φ UMa using the MPIA MAGIC

infrared camera system are shown in Figure 16. The use of ALFA resulted in significant increases in the peak intensity with a corresponding increases in the Strehl ratio.



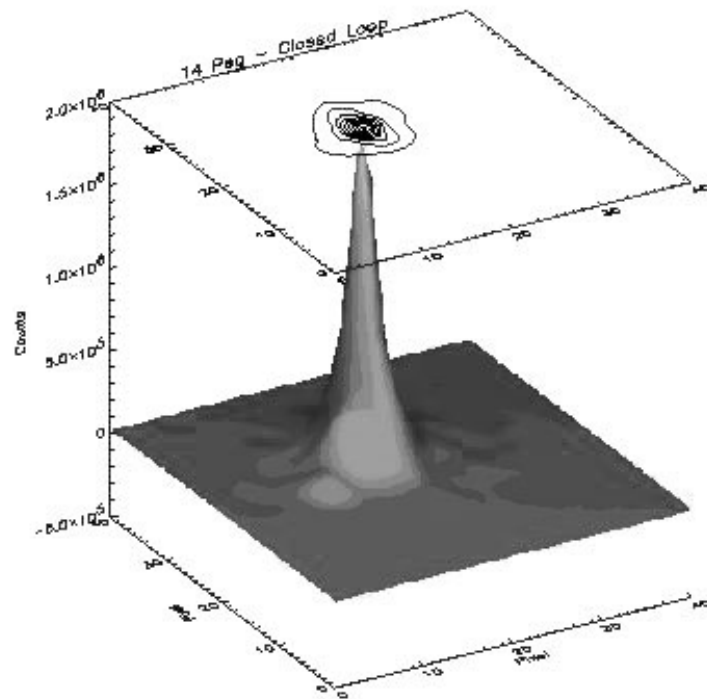
14 Peg with ALFA
and MAGIC
Calar Alto 21 July 1997

Images taken at a wave-length of 2.2 microns. The total integration time was 20 seconds (100 images 0.2 seconds each).

Pixel scale: 0.056 "/pixel

FWHM without ALFA:
~0.85 arcsec

Strehl: ~2.4%



FWHM with ALFA:
~0.2 arcsec

Tip-tilt loop: 80 Hz

AO loop: 100 Hz

Modes corrected: 15

Strehl: ~20%

Strehl improves by a factor of approx. 8.3 from uncorrected to corrected image

Figure 16. Recent results from the ALFA system.

The ultimate goal for the ALFA system is the use of the sodium layer guide star as the source for the control system. In an observing run in early December, closed loop operation was first achieved with the laser source. The laser guide star has an equivalent brightness of a

10 magnitude star. ALFA provided stable correction at a 60Hz frame rate with useful improvement in image quality. Performance with the laser source is chiefly limited by the detector noise of about 10 electrons per pixel. A full analysis of the system performance relative to theory and model predictions is still in progress. Some preliminary results pertaining to the control loop performance are presented below.

Figure 17 shows the magnitudes of the open loop and closed loop spectra of the focus mode computed from 20 second data segments (6000 frames). As expected, there is significant attenuation of the disturbance below 10 Hz. Figure 18 shows the transfer function computed from the spectra shown in Figure 17 and compares it with the theoretical closed-loop transfer function (see also Figure 15).

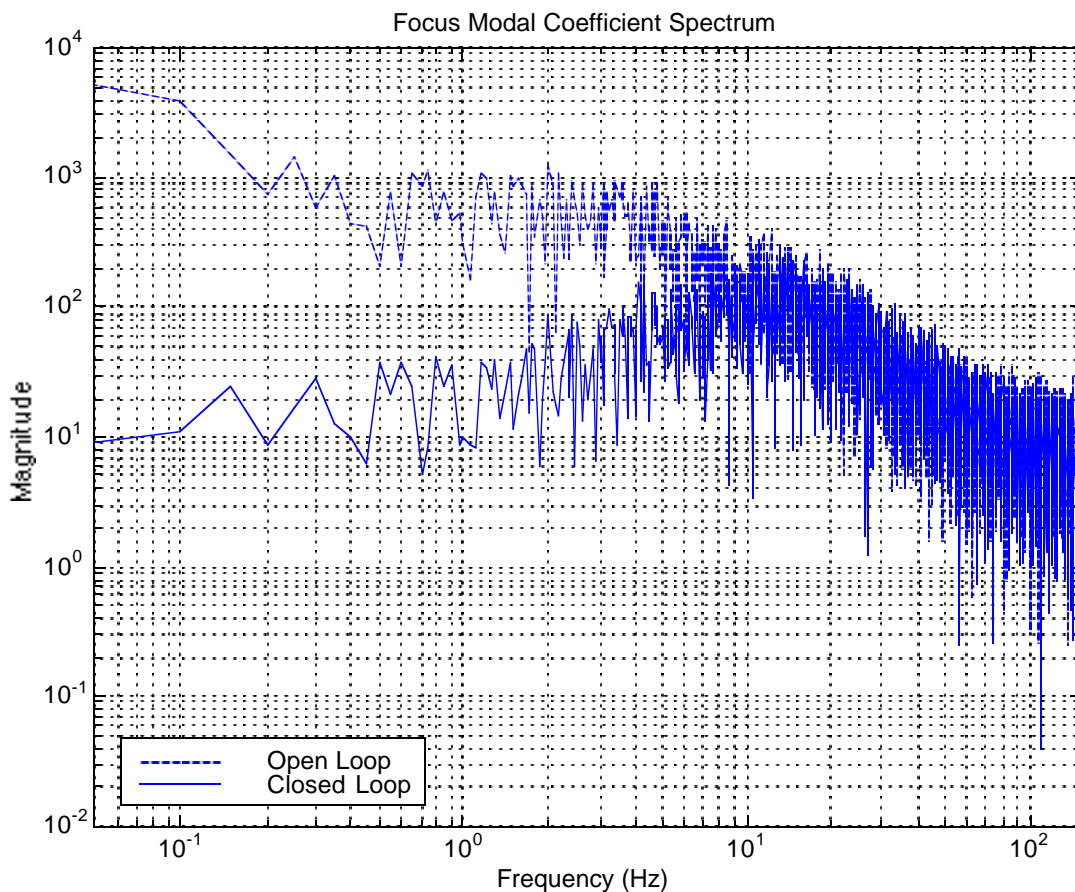


Figure 17. Spectra of focus mode coefficients with adaptive optics loop open and closed.

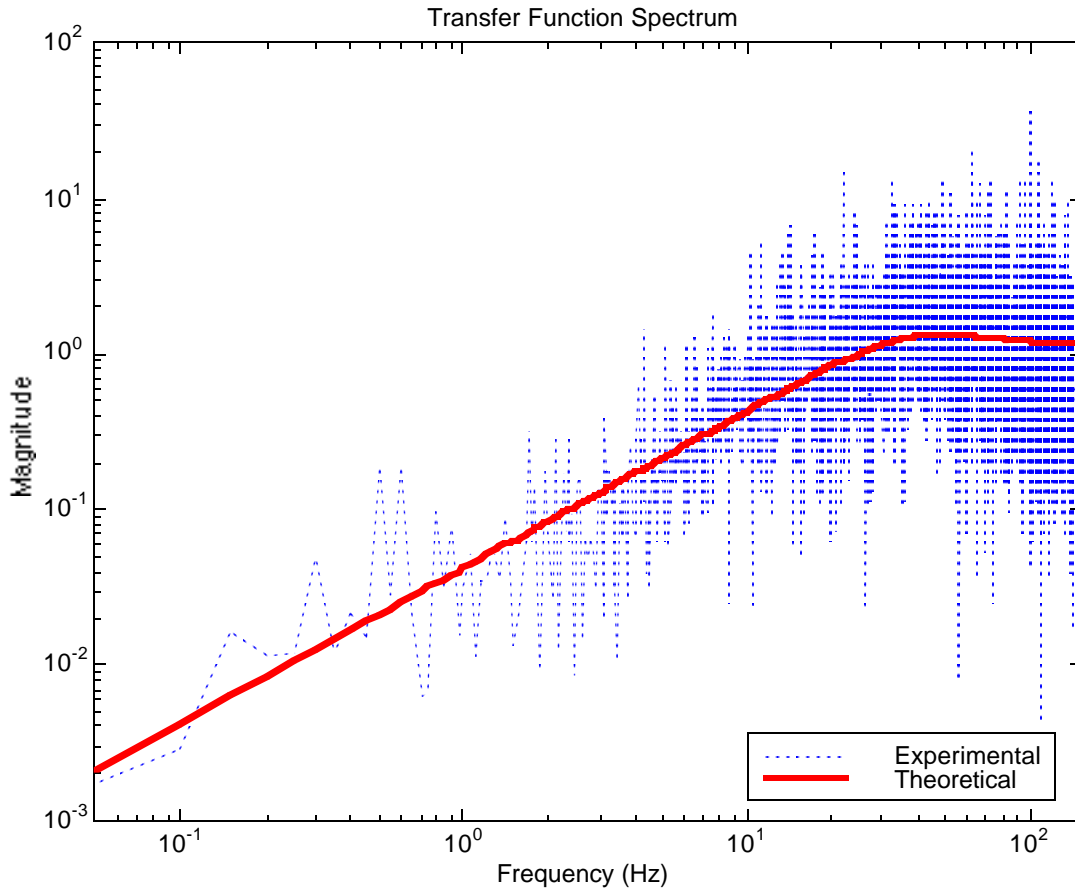


Figure 18. Transfer function computed from observed data.

4. Real-time modal control processor (RTC)

4.1 Hardware implementation algorithm

In many adaptive optics systems, a single matrix multiply is used to convert wavefront slopes to actuator control signals^{8,9}. As discussed in detail in Section 3, in order to accommodate the varied requirements, we chose to divide the wavefront reconstruction into two parts. A schematic for the wavefront control is shown in Figure 6.

The wavefront is first reconstructed and then projected into Zernike modes in the box marked, 'Modal Reconstructor'. The Modal Offsets junction applies both an additive offset

and a weighted filtering function to the reconstruction. These modal weights can be computed off-line, and can be changed at any time. Another matrix multiply is performed in the Modal Injection box in order to convert the filtered modes into actuator commands for the deformable mirror.

4.1.1 Hardware implementation

All matrix operations are implemented in the RTC via 5 digital signal processor (DSP) boards with each board containing 4 DSP chips thus making a total of 20 DSP processors in which to distribute all required calculations. The DSP chips are allocated to each operation according to the table below.

Table 3: Allocation of wavefront control functions in a DSP based processor

<u># DSP's</u>	<u>Operation</u>
5	camera input, gain, offset
8	gradients (2 algorithms)
4	reconstruction/modal projection
1	compensation (weighting)
2	modal injection/DM output

This implementation is capable of projecting 50 wavefront control modes in 833 μ s execution time. The mathematical operations for this processor are capable of being scaled to 349 actuators by adding more DSP boards. A photograph of the RTC is shown in Figure 19. The DSP boards are housed in a VME based card cage. The five boards share data via the connecting cables in the front. The two boards at the left are for external communications.

4.2 Software considerations

The RTC has been programmed to interact with the entire adaptive optics system both in real-time and for off-line studies. In real time the RTC performs its wavefront control

function, and off-line it provides wavefront information for atmospheric studies and to determine, for instance, an optimal set of weights for modal control. In real-time, the RTC is programmed in C, and takes instructions from a Motorola 68060 running the real-time VxWorks¹⁰ operating system. For off-line studies the RTC takes instructions relayed by EPICS (Experimental Physics Industrial Control System)¹¹, a client/server model distributed database. EPICS has the ability to communicate between VxWorks and our host computers. The top layer of control between the RTC and the rest of the adaptive optics system is shown in Figure 20. The RTC is contained within the ellipse marked 'AO Loop'.

Figure 21 shows how off-line queries are handled by the RTC. A data manager sends requests to the real-time interface which then returns the requested data. This information is input into WAVELAB, AOA's commercially available software package for Shack-Hartmann data analysis. WAVELAB contains a library of C language routines all of which can be called on a command line or embedded into a script via the Tcl language. Both Tcl and its graphical language, Tk¹², are used to write specialized data analysis procedures for analyzing atmospheric data. The results of these analyses are then sent back through the data manager and the real-time interface so that weights can be modified in the RTC.



Figure 19: Wavefront control processor box shown in lower right along with one of the authors (JN).

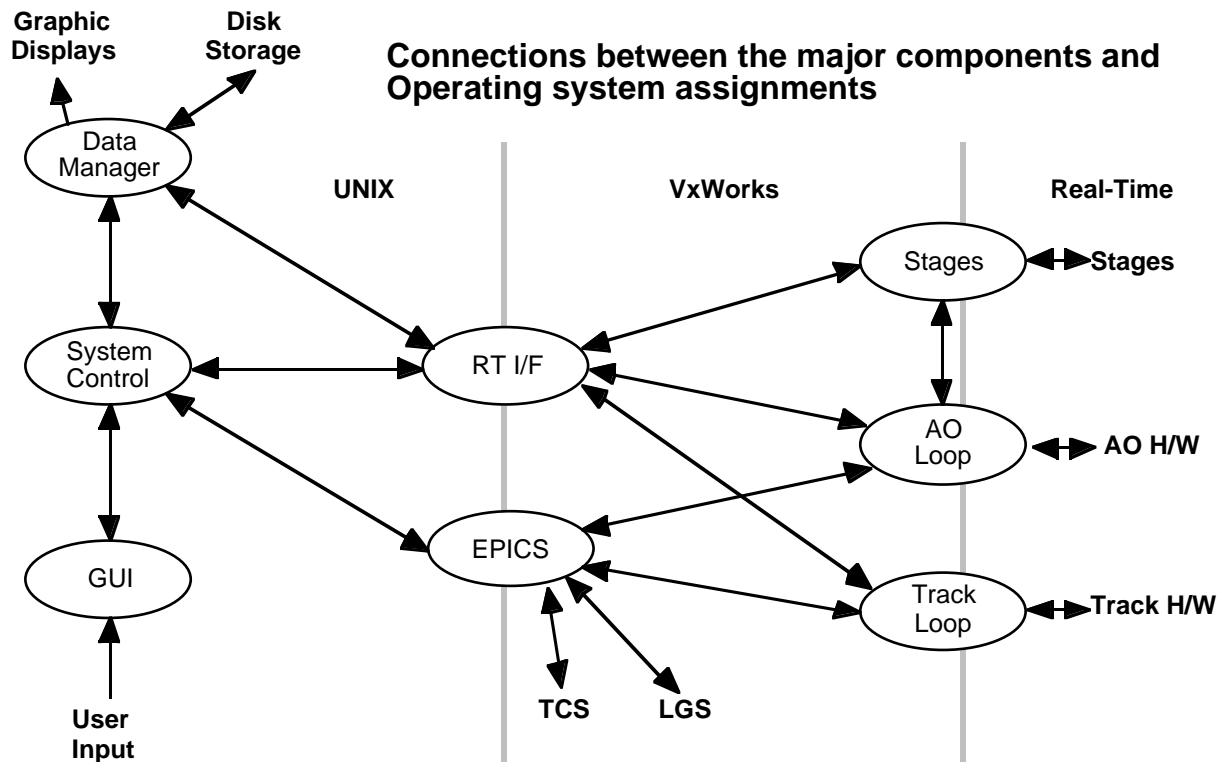
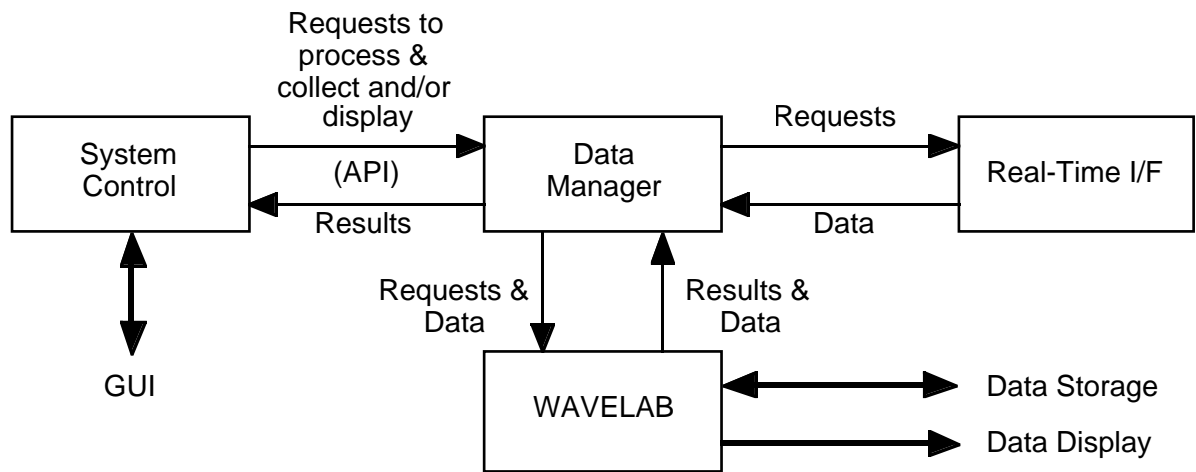


Figure 20: Top level of software control between the RTC and the entire adaptive optics system.



Data Manager

- Tcl level access
- Interface to data analysis, storage, & display
- Handles data transfer between the System Control, Real-Time subsystems and WAVELAB

WAVELAB

- AOA Wavefront analysis package
- Perform data storage, replay, and display
- Data reduction routines

Figure 21: Data flow diagram for obtaining off-line data from the Wavefront control processor.

5. Summary

A flexible wavefront control processor was built and integrated by AOA for a sodium laser guide star adaptive optics system to be located on a 3.6m telescope located in Calar Alto, Spain, and operated by the Max Planck Institute for Astronomy-Heidelberg. The processor was built in response to requirements for an adaptive optics system that would need to operate over varied conditions, and could be upgraded at a modest cost. The processor is able to perform modal wavefront control by a two matrix multiply approach, and has the ability to accommodate varying wavefront sensor geometry, system bandwidths, and atmospheric weights. This processor was built from commercial DSP boards. Its software is written to interact with both real-time and off-line requests and makes use of widely supported commercial and public domain software tools.

Acknowledgment

The authors would like to acknowledge the help of the whole of Team ALFA, both at AOA and at MPIA. The work reported here was funded by MPIA and by NSF Contract #ECS-95-10449.

- 1 . J. Beckers, "Adaptive Optics for Astronomy: Principles, Performance, and Applications", *Ann. Rev. Astr. & Astrophys.* **31**, pp13-62 (1993).
- 2 . A. Wirth, F. Landers, B. Trvalik, J. Navetta, and T. Bruno, (1995), 'A laser guide star atmospheric compensation system for the 3.5m Calar Alto telescope', Vol. 23 of 1995 OSA Technical Digest Series (Optical Society of America) paper MA3-1.
- 3 . R.J. Noll, 'Zernike polynomials and atmospheric turbulence', *J. Opt. Soc. Amer.* **66**, p207-211 (1976).

4. J.Y. Wang and D.E. Silva, (1980), 'Wave-front interpretation with Zernike polynomials', *Applied Optics*, **19**(9), p1510-1518.
5. Andreas Glindemann, McCaughran, M.J., Hippler, S., Wagner, C., Rohloff, R.-R., "CHARM: A Tip/Tilt Tertiary System for the Calar Alto 3.5m Telescope". OSA Summer topical meeting on Adaptive Optics, Maui July 8-12 1996.
- 6 J. Huang, D. P. Looze, N. Denis, D. Castanon, and A. Wirth, "Modeling and Identification of Adaptive Optics Systems," submitted to *International Journal of Control*.
- 7 Franklin, G. F., J. D. Powell, and A. Emami-Naeini, *Feedback Control of Dynamic Systems*, Addison-Wesley, 1988
- 8 Rousset, Gerard; Beuzit, Jean-Luc; Hubin, Norbert; Gendron, Eric; Madec, Pierre-Yves; Boyer, Corinne; Gaffard, Jean-Paul; Richard, Jean-Claude; Vittot, M.; Gigan, Pierre; Lena, Pierre J. 'Performance and results of the COME-ON+ adaptive optics system at the ESO 3.6m telescope', *Proc. SPIE*, **2201**, p1088-1095, "Adaptive Optics in Astronomy", Mark A. Ealey; Fritz Merkle; Eds.
- 9 . Beuzit, Jean-Luc; Hubin, Norbert; Gendron, Eric; Demailly, Laurent; Gigan, Pierre; Lacombe, Francois; Chazallet, F.; Rabaud, D.; Rousset, Gerard. (1995), "ADONIS A user-friendly adaptive optics system for the ESO 3.6m telescope", paper MC1-1 in presented at the OSA topical meeting on Adaptive Optics, 2-6 October 1995, Garching, Germany. printed in 'Adaptive Optics, 1195 Technical Digest Series, Volume 23.
10. VxWorks is a product of Wind River Systems, Inc., 1010 Atlantic Avenue, Alameda, CA 94501.
- 11 . EPICS is free to non-profit and government sites from Los Alamos National Laboratories, and is commercially available from Kinetic Systems, Corp., 7308 South Alton Way Bldg 2, Engelwood, CO 80112.

12 . Both Tcl and Tk are freely available in the public domain. For further information on these languages, see Brent B. Welsh, (1995), Practical Programming in Tcl and Tk, Prentice Hall PTR, Upper Saddle River, NJ.